Horizon 2020 Grant Agreement no: 814523

Terahertz end-to-end wireless systems supporting ultra-high data Rate applications

ThoR

D4.5

TWTA

Coordinator (EU): Thomas Kürner
Organisation: Technische Universität Braunschweig

Coordinator (Japan): Tetsuya Kawanisihi
Organisation: Waseda University

Start date of project: 01-Jul-2018

Date of issue: 09-SEP-2021
Due date: 31-MAR-2021
Ref: ThoR_WUT_210714_B_WP4

Leader in charge of deliverable: Tetsuya Kawanishi
Waseda University

Project co-funded by the European Commission within the Horizon 2020 programme and the National Institute of Information and Communications Technology in Japan (NICT)		
Dissemination level		
PU	**Public**	**X**
PP	**Restricted to other programme participants (including the Commission Services)**	
RE	**Restricted to a group specified by the consortium (including the Commission Services)**	
CO	**Confidential, only for members of the consortium (including the Commission Services)**	

Contents

Change register

Version	Date	Author	Organisation	Changes
A	14-7-2021	Tetsuya Kawanishi Kunio Tsutaki	Waseda University	Initial
B	25-7-2021			

Reviewed by Guillaume DUCOURNAU IEMN-CNRS, Univ of Lille A July-20th-2021

1. Statement of independence

The work described in this document is a genuine result of efforts pertaining to the ThoR project. Any external source was referenced properly.

Confirmation by Authors: Tetsuya Kawanishi Waseda University
Kunio Tsutaki Waseda University

2. ABBREVIATIONS

CW	Continuous wave
CST	Electromagnetic simulation software of the Dassault Systems Deutschland GmbH
FWG	Folded waveguide
LIGA	Lithographie, Galvanoformung, Abformung
MEMS	Micro electromechanical system
PIC	Particle in cell
SPring-8	Super photon ring-8 GeV
SWS	Slow wave circuit
THz	Terahertz
TWT	Traveling wave tube
TWTA	Traveling wave tube amplifier
VNA	Vector Network Analyser
5G	5th Generation Mobile Communication System

3. Executive summary

This deliverable provides the results of a TWTA prototype. Our goal is to provide TWTA for the extension of the THz wireless communication distance. TWTA is an RF power amplifier used in the final stages of the radio transmitter. The prime components of the TWTA are the TWT device itself and the high-voltage power supply. To achieve the required specifications, especially the gain characteristics around the central frequency of 290 GHz, improvements to the TWT device have been performed. We evaluated the preliminary prototype of the TWT device and clarified the technical challenges. Thereafter, we improved TWT design. To increase the gain of the TWT, we focused on the electron trajectory distribution when electrons passed through the electron beam hole of the FWG-SWS. We also tried to reduce the manufacturing errors of the amplifying element of the TWT device. Further, the MEMS manufacturing process was improved to reduce the surface roughness of the amplification element. In addition, the amplification element is resistant to deformation. Finally, the prototype of the TWT device was fabricated using a newly designed amplification element. We evaluated the TWT prototype and examined the technical issues in achieving the goal.

4. Introduction

In recent years, wireless communication networks have been facing a rapidly increasing demand for applications that requires higher data rates. To meet this demand, research has been undertaken worldwide to expand the carrier frequency from the microwave range to the millimetre wave range in wireless communication links. Realisation of a high-power and wide-band device for a transmitter in terahertz regions is one of the solutions for super high-data-rate wireless communications beyond 5G. The TWT device is a key element in telecommunications, satellite transmitters, military radar, electronic countermeasures, and communication data links with high power. The power gain of the TWT device product in the Q/V band is on the order of 50 dB, and the radio frequency (RF) output power reaches 150 W in CW operation mode [1].

Our 300-GHz-band TWT device is based on the technology of a millimetre-wave TWT device, which is a vacuum tube that is used to amplify the RF signal using a slow-wave circuit structure (SWS) as an amplifying element. Figure 1 shows the basic structure of 300-GHz-band TWT. The electron beam, which travels in a straight line in the SWS, is generated by an electron gun. The spent electron beam is collected on the other side of the TWT. The 300-GHz signal is input from the RF port, which then travels in the SWS. The signal is amplified via the interaction with electrons.

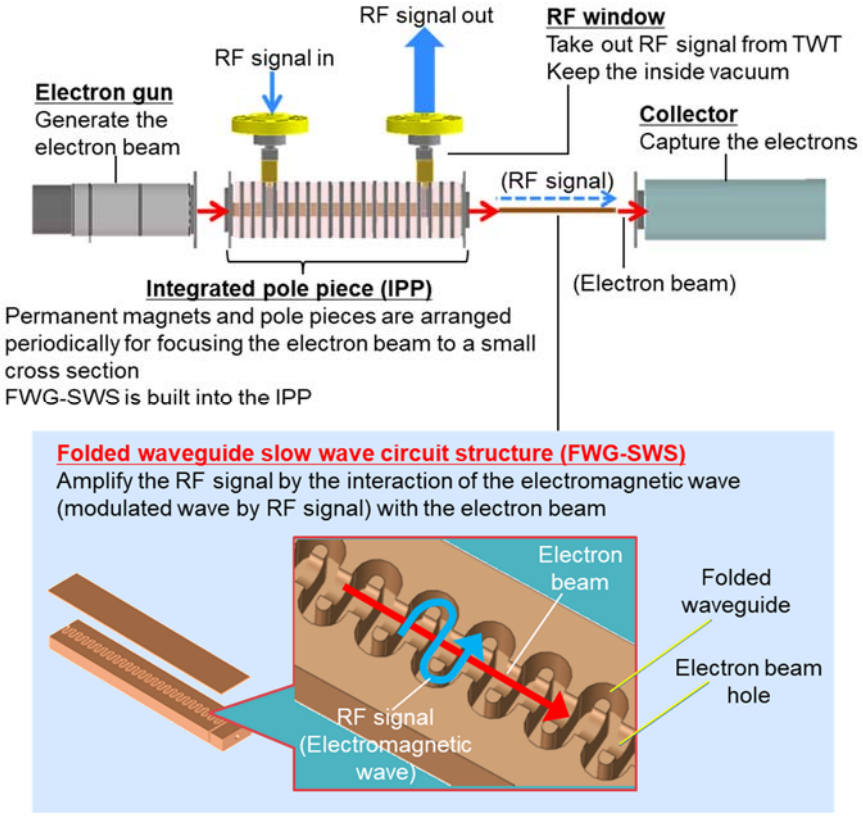

Figure 1. Illustrative sketch of the 300-GHz-band TWT device.

Helix-SWS is used for TWT device products up to the Q/V band; however, helix-SWS does not operate in the terahertz region. This is because the diameter becomes too small to be fabricated in a vacuum tube with high precision. Therefore, we have been actively developing a folded waveguide SWS (FWG-SWS) [2],[3]. Thus, our 300-GHz-band TWT device also employs an FWG-SWS as an amplifying element. The latest MEMS technology was used to fabricate the FWG-SWS because it is necessary to create a fine and deep pattern. The FWG pattern is several centimetres long, and its width is less than 1 mm. The RF signal wave travels in the FWG and the electrons emitted from the cathode travel in a straight circular hole.

As shown in Table 1, the major targets of the 300-GHz-band TWT are an output power greater than 1 W and a gain larger than 20 dB in a specific 5-GHz bandwidth in the frequency range of 280–300 GHz. Considering the production variations and other aspects, a wider operating voltage range of 12–15 kV and a beam current range of 5–15 mA were set to achieve an output power of 1 W or greater, as shown in Table 2. Furthermore, for a compact and lightweight TWT, a periodic permanent magnet (PPM) is employed for electron beam focusing in SWS.

Table 1. Target value

Item	Value
Frequency Range	280–300 GHz
Output Power	> 1 W
Gain	> 20 dB
-3dB Bandwidth	> 5 GHz

Table 2. Operating Parameter

Beam Voltage	Beam Current	Collector Voltage
12–15 kV	5–15 mA	4 kV

5 TWT design

5.1 Design theory of the FWG-SWS

In this chapter, the design theory of FWG-SWS is presented, which was then applied to the concrete design of the broadband FWG-TWT in the 300-GHz range. Next, the first trial TWT was built based on the design, and the evaluation results are shown. Furthermore, the evaluation results of the trial TWT have been analysed, and measures to solve the problems are discussed.

Figure 2 shows the cross-sectional structure of the FWG-SWS with each dimension labelled. In this figure, a and b represent the width and height of the rectangular waveguide, respectively, $p(=2b)$ is pitch, ℓ is straight length from the centre axis, L $(=\pi p/2+2\ell)$ is path length of the RF wave per pitch, and r_d is the radius of the electron beam hole.

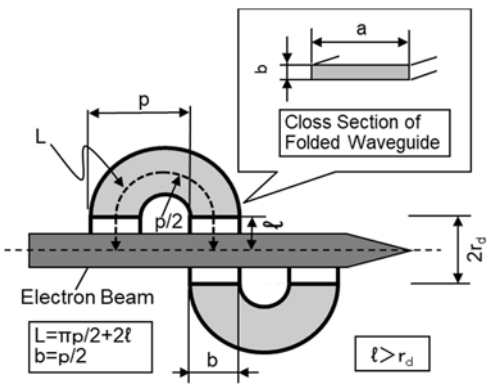

Figure 2. Cross-sectional structure of FWG-SWC.

In general, the propagation characteristics of the SWS can be described using three circuit parameters: phase velocity, coupling impedance, and RF loss. Therefore, theoretical equations for the phase velocity v_p, coupling impedance Z_c, and RF loss L_c are very useful for studying the TWT optimisation design. Theoretical equations of phase velocity and coupling impedance for the FWG-SWS were introduced in previous papers [4], except for the RF losses.

Phase velocity is expressed as

$$\frac{v_p}{c} = \frac{2p}{2L\sqrt{1-\left(\frac{\lambda}{\lambda_c}\right)^2}}, \quad L = \frac{\pi p}{2} + 2\ell \qquad (1)$$

where c is the light speed, L is total waveguide length, λ is wavelength, λ_c is cut-off wavelength, and ℓ is straight length shown in figure 2.

Coupling Impedance Z_c can be calculated using

$$Z_c = \frac{C_{gap}\left(\frac{2b}{a}\right)\eta}{\sqrt{1-\left(\frac{\lambda}{\lambda_c}\right)^2}} \qquad (2)$$

$$C_{gap} = \left\{\left(\frac{1}{\beta p}\right)\frac{\sin\left(\frac{\beta b}{2}\right)}{\frac{\beta b}{2}}\right\}^2, \quad \beta b = \frac{2\pi f b}{v_p} \qquad (3)$$

where f is the frequency and η is the intrinsic impedance which is approximately 377 Ω for free space.

In the 300-GHz band, the effect of RF loss cannot be ignored. In this deliverable, we introduce a simple equation for the RF loss L_c of the FWG-SWS, which is theoretically obtained from the attenuation constant of the rectangular TE_{10} waveguide mode.

$$L_c = 8.68\frac{L}{p}R_s\frac{1+\frac{2b}{a}\left(\frac{\lambda}{\lambda_c}\right)}{b\eta\sqrt{1-\left(\frac{\lambda}{\lambda_c}\right)^2}} \quad [dB/\lambda g] \qquad (4)$$

In equation (4), R_s is the skin effect surface resistivity, which is expressed as (for copper)

$$R_s = 2.61\times10^{-7}\sqrt{f} \quad [\Omega\cdot m] \qquad (5)$$

The design to achieve a wider bandwidth for the 300-GHz-band TWT was investigated by using theoretical analysis of three circuit parameters and the classical large signal simulation code [5], which has been practically used for helix TWT designs. The classical simulation code is very useful for the simple design of FWG-TWT. Further, in the simulations of the 300-GHz-band FWG-TWT, the disc model for the electron beam and first-order circuit equations were used. In addition, stable operation and good electron beam transmission were considered for the practical use of the TWT.

5.2 Design approach for wideband FWG-TWT in the 300-GHz range

The TWT must have a wide band characteristic with an instantaneous bandwidth of 5 GHz or greater in the frequency range of 280–300 GHz for high-speed communication. Here, the design theory in the previous section is used to design the FWG-SWS to realise wideband amplification of 5 GHz or greater.

In figure 3, the phase velocity calculated using equation (1) for the three types of FWG-SWS is represented by the phase difference βp per pitch. In addition, three 12-kV beamlines are shown. This diagram, which is commonly referred to as the ωβ diagram, can be used for optimizing the FWG-SWS structure. To maximize the interaction between the electromagnetic-wave in the FWG and the electron beam in the hole, the speed of the electron beam should be slightly faster than that of the electromagnetic-wave. Therefore, we have designed the electron beam and electro-magnetic wave to synchronize in a frequency lower than the central frequency of the desired operation range. For example, the frequency of the speed synchronization should be around 280GHz, to achieve wideband operation in 280-300 GHz (centre frequency is 290 GHz). In figure 3, the ωβ-1 FWG-SWS has a phase difference of 1.3π per pitch synchronised with the 12-kV beamline at a frequency of 280 GHz, while ωβ-2 has a phase difference of 1.45π, and ωβ-3 has a phase difference of 1.6π. Among the three types of FWG-SWS, it is evident that ωβ-3 maintains a synchronous relationship over a wider frequency range of circuit waves and electron beams.

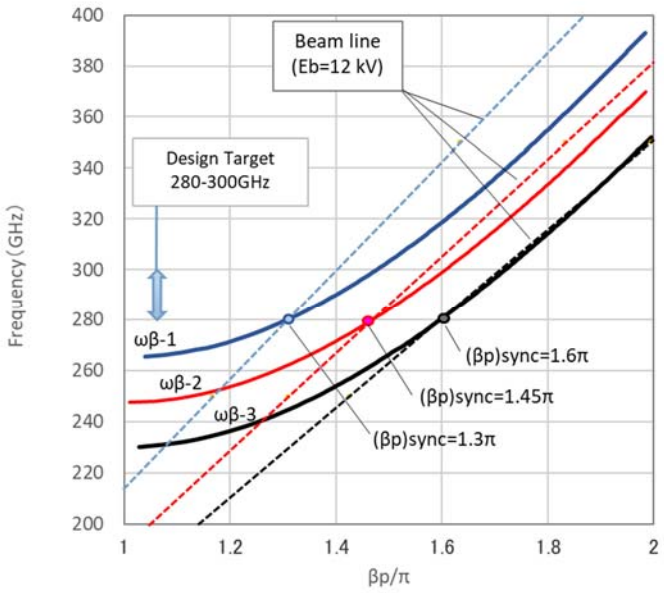

Figure 3. ω-β diagram of 3 types design examples for 300 GHz TWT

Figure 4 shows the frequency characteristics of the small signal gain (SSG) for the three types of FWG-SWS. The classical simulation code was used to facilitate simple calculation of the SSG of the TWT. In the figure, each beam voltage is set to have the same synchronisation relationship at a frequency of 290 GHz. The gain of the FWG-SWS of ωβ-1 is as high as 30 dB or greater, but the bandwidth is extremely narrow. In contrast, ωβ-3 has a low gain, although the gain is obtained in the wide frequency range of 280–300 GHz. It can be observed that the synchronisation relationship was maintained over a wider frequency range.

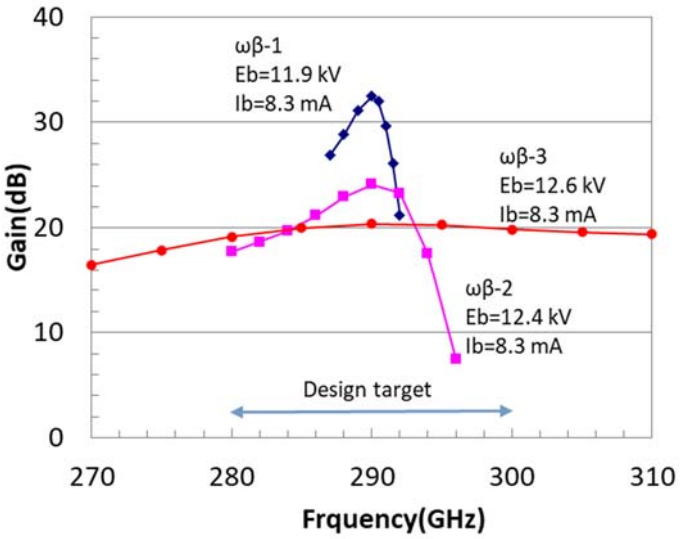

Figure 4. Frequency response of the gain for 3 types design examples for 300-GHz-band TWT centred at 290 GHz.

From the above results, it is possible to realise a wideband FWG-TWT with an instantaneous bandwidth of 5 GHz or greater by setting (βp) sync to a large value, however, the reduction in gain must be considered.

To realise an instantaneous bandwidth of 5 GHz or greater, we decided to finally adopt ωβ-3 from the three types of FWG-SWS, and the detailed structural dimensions of FWG-SWS using ωβ-3 are shown in Table 3. Further, certain detailed operation analysis results of the 300-GHz band TWT that adopted the ωβ-3 FWG-SWS are shown as well.

Table 3. Dimensions of 300 GHz FWG-SWS

Parameter	Label	Value
Width of FWG	a	0.651 mm
Height of FWG	b	0.091 mm
Pitch	p	0.182 mm
Beam hole radius	r_d	0.109 / 0.123 mm
Straight length/2	ℓ	0.137 mm
Total SWC length	L_{eff}	26.7 mm
Total pitch Number	N	146

Figure 5a shows ω-β diagrams of the theoretical equation (1) and the simulation using the CST Studio Suites with four beam lines (12, 13, 14, and 15 kV). For the beam lines**,** the relativistic effects were considered. Figure 5b shows ω-β Diagrams in 260-320 GHz with βp 1.4-1.8. In this figure, good agreement for both ω-β diagrams around the operation band was observed. For the broadband operation in the range 280–300 GHz, the electron beam and the electromagnetic wave were

synchronized at a large value of βp(□1.6π).

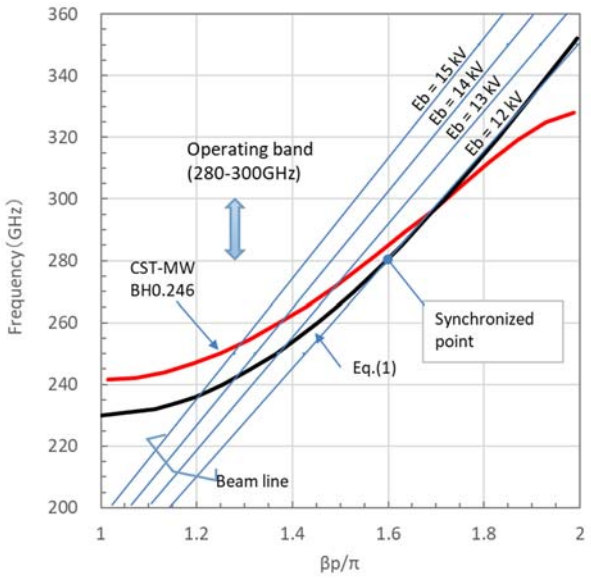

Figure 5a. ω-β Diagrams of the FWG-SWC and beam lines

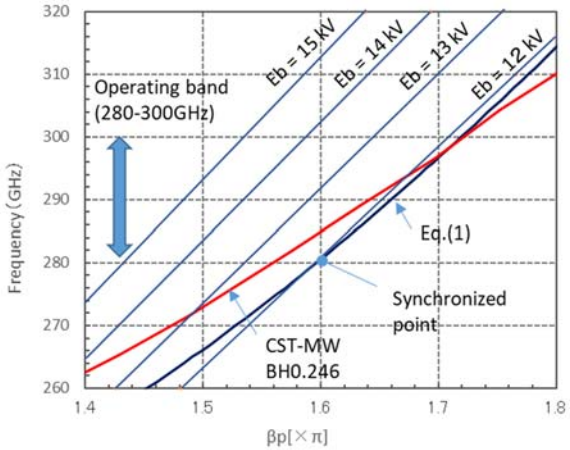

Figure 5b. ω-β Diagrams in 260-320 GHz with βp 1.4-1.8.

Figure 6 shows calculation results of the coupling impedance Z_c and RF loss L_c of the 300-GHz-band FWG-SWS. Z_c and L_c at the centre of operating band are 3.4 Ω and 0.044 dB/λ_g, respectively. These appear to be the appropriate value as input data for further large signal simulations.

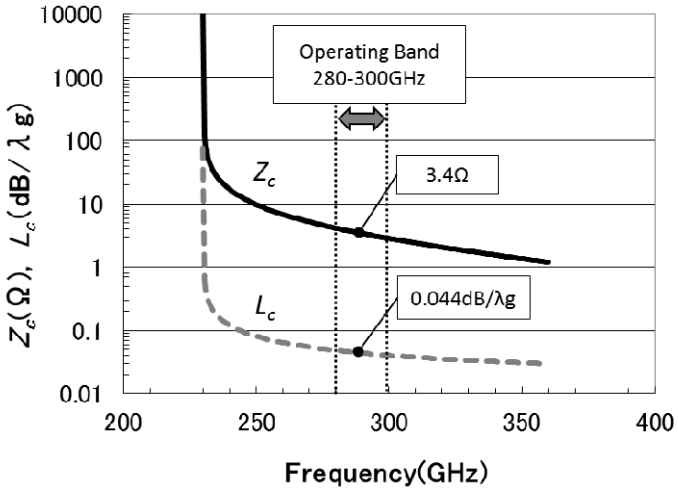

Figure 6. Coupling impedance and RF loss as a function of frequency

Figure 7 shows simulation results of gain, beam efficiency η_b, and RF loss η_{loss} as a function of axial distance. At output position z=26.7 mm, beam efficiency of 2.7 % and large signal gain of 20.2 dB were obtained. Further, the RF loss of TWT was 22 % of the RF energy transferred from the electron beam.

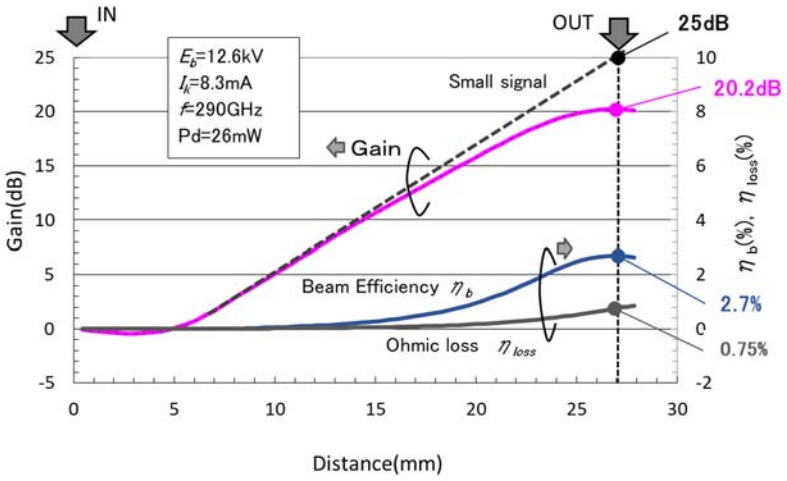

Figure 7. Simulation results of gain, beam efficiency and RF loss as a function of axial distance.

Figure 8 shows simulation results of gain and beam efficiency at output position (z=26.7 mm) as a function of frequency, where the gain is about 20 dB in the range 280–300 GHz The output power is greater than 2 W (correspond to the beam efficiency of 2%).

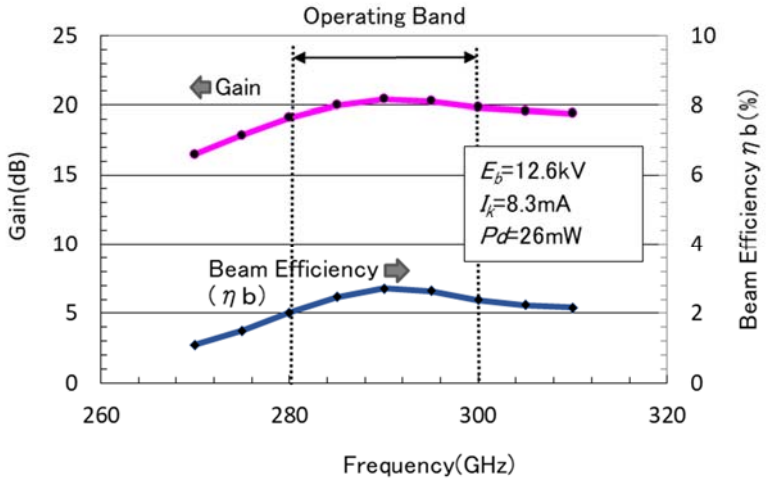

Figure 8. Simulation results of gain and beam efficiency at output position (z=2 6.9 mm) as a function of frequency.

5.3 Preliminary study

We evaluated the TWT device to conduct a closer study of the theoretical design. The TWT was designed to satisfy the values listed in Table 1 using theoretical calculations. TWT devices were prototyped before the ThoR project began. The TWT device was subjected to aging, therefore, as shown in figure 9, an ion pump was used to maintain the interiors of the TWT device in ultra-high vacuum. In addition, the VNA extension modules were connected to the WR-3 ports of the TWT device.

Electrical adjustments must be performed after the TWT device assembly is completed. In addition, because the transmittance of the electron beam is low, stable operation cannot be performed in the CW mode. After electrical adjustments, the transmittance of the electron beam increases while adjusting the trajectory of the electrons. To protect against internal local heating damage that occurs when the TWT becomes unstable, electrical adjustments were made in the pulse mode as shown in Figure 10.

When the waveform of the pulse generator becomes high, the electron beam can be passed by applying a voltage to the anode electrode of the TWT device. Simultaneously, a trigger signal is sent to the VNA to start the measurement.

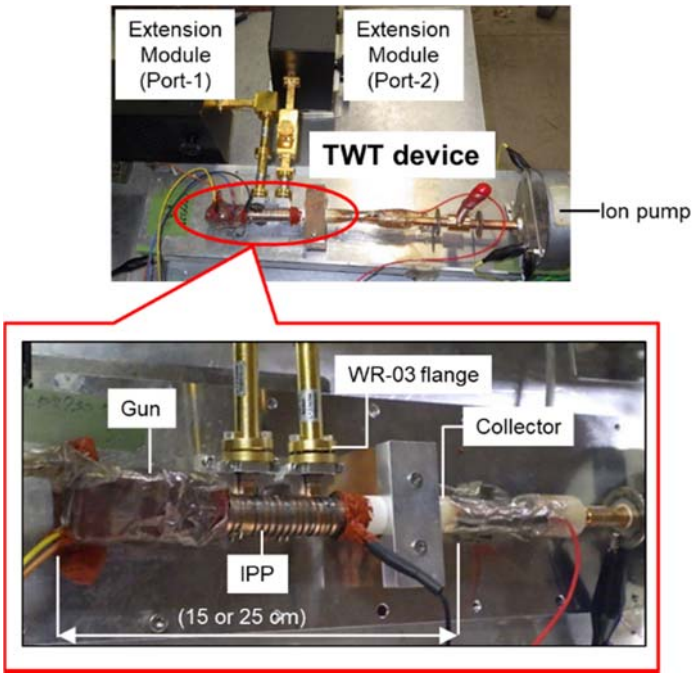

Figure 9. First prototype of the TWT device.

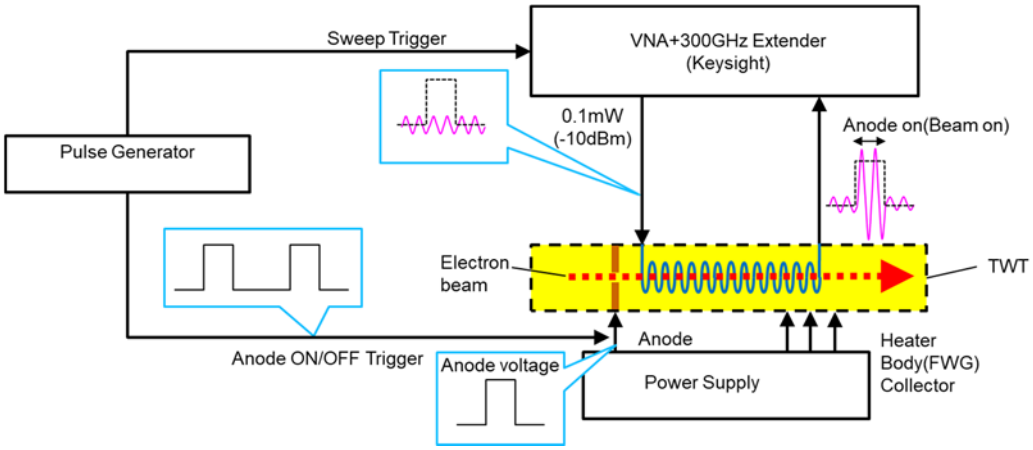

Figure 10. Measurement under pulse operation.

In figure 11, S21 is a scattering parameter from port-1 to port-2, which corresponds to the system gain of the TWT device. The peak frequency moved to the left when the applied voltage of the FWG-SWS increased. However, the peak value of the gain decreased as the frequency increased because the coupling between the RF signal wave and the electron beam weakened. Further, the frequency bandwidth also increased with the increase in frequency. These results are consistent with the results from the TWT design theory described in the previous section. From the figure, we find a gain of approximately 7 dB at a frequency of 260 GHz when 15 kV was applied to FWG-SWS. However, in the target frequency range of 280–300 GHz, the system gain of the TWT device was still negative. The RF output from the TWT device did not reach the saturation point because the RF input power was low (−10 dBm). Therefore, the major problem with this TWT is the weak coupling between the RF signal wave and the electron beam.

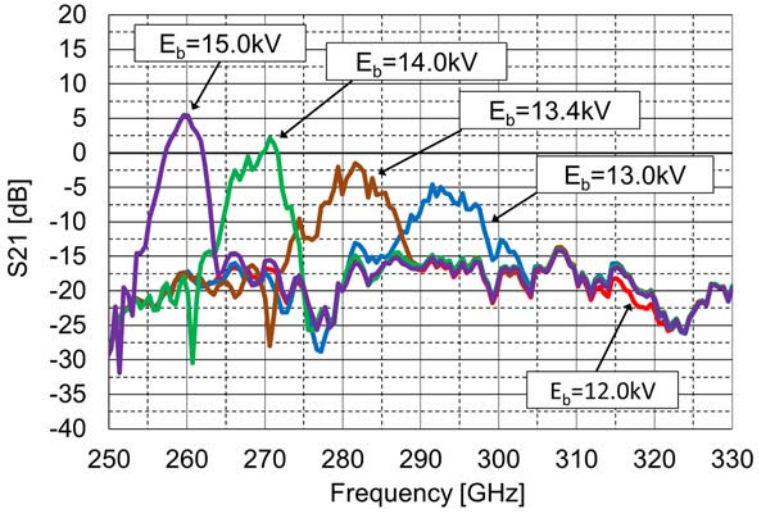

Figure 11. Frequency responses of the TWT device with a built-in single-FWG-SWS (Pulse mode).

Next, to increase the TWT gain easily, we assembled a double-FWG-SWS TWT device. Two FWG-SWSs were coupled in series (figure 12). In figure 13, it can be observed that a TWT gain of 14 dB was obtained at a frequency of 265 GHz when 14 kV was applied to the FWG-SWS. Because the FWG-SWS is divided, the measured S21 in the frequency range where the circuit wave and electron beam are not synchronised should be infinitesimal, thus, the base line of S21 in figure 12 appears to indicate the noise level.

By adopting double FWG-SWS, we could confirm the increase in gain, but we have not yet achieved a target gain of 20 dB.

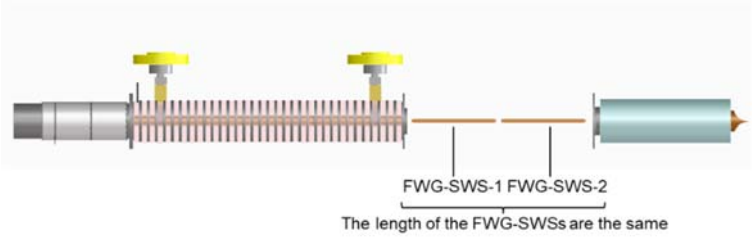

Figure 12. Illustrative sketch of the TWT device with a built-in double-FWG-SWS.

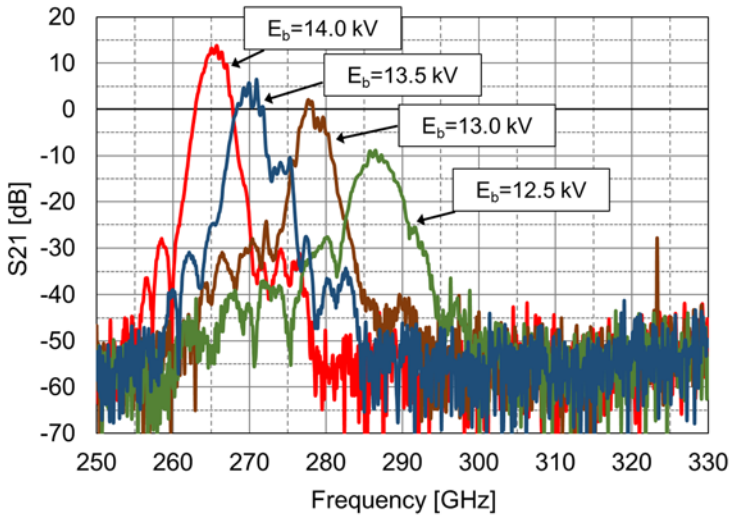

Figure 13. Frequency responses of the TWT device with a built-in double-FWG-SWS (Pulse mode).

5.4 Design improvement of the TWT device

It is important to investigate the cause of the large deviation in the measured gain of the prototype TWT from the calculated value predicted based on the design theory when considering future measures.

5.4.1 Cause analysis of low gain in experimental results

The design theory ignores the effect of the beam hole on the phase velocity. Therefore, here, the ωβ diagram, based on equation (1), was compared with the ωβ diagram of FWG-SWS considering the beam hole using CST-MW. Figure 14 shows a CST-MW ωβ diagram of the 300-GHz-band FWG-SWS for three types of electron beam hole radii. The passband becomes narrower as the electron beam hole radius increases, but in the operating band, equation (1) is almost the same as CST-MW.

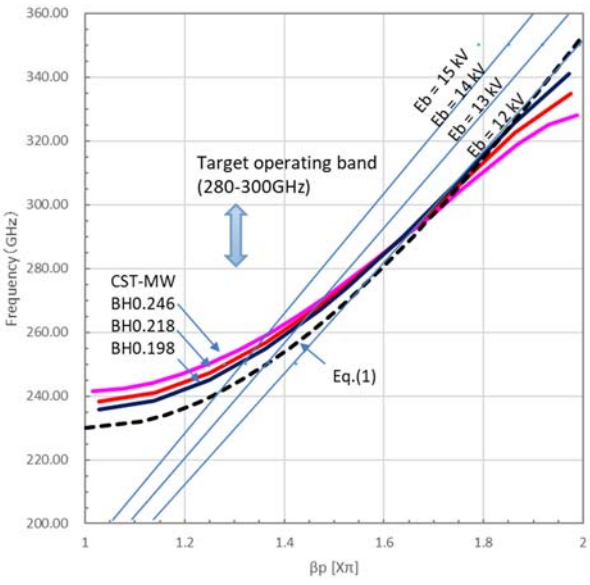

Figure 14. ω-β Diagrams for beam holes as a parameter and beam lines

Figure 15 shows the calculation result of the RF loss using equation (4), the results using CST-MW, and the measured value. For equation (4), the calculated value was doubled considering the surface roughness. The measured value of FWG-SWS with a beam hole radius of 0.198 mm was approximately

− -16 dB at 280-300 GHz, which was in good agreement with the CST-MW. In addition, equation (4), which ignores beam holes, is also at a level that can be used for design by making a double correction.

For the 300-GHz-band FWG-SWS, three circuit parameters were corrected by comparing the results of the theoretical equations (1) to (4) with CST-MW and the measured values. Subsequently, the operation analysis of the TWT by classical simulation code was performed using the result.

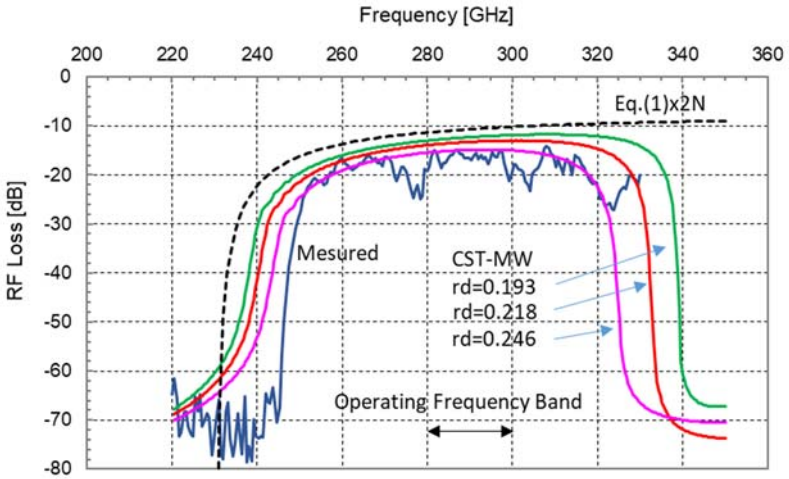

Figure 15. Comparison of measured RF Loss, RF loss by equation (1) and CST-MW

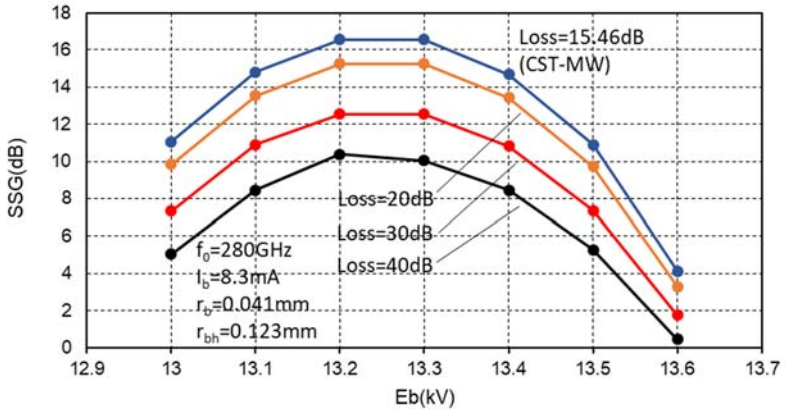

Figure 16. Small signal gain versus beam voltage for the RF Loss as a parameter

Figure 16 shows the dependence of the small signal gain (SSG) on the beam voltage with RF loss as a parameter. in the calculations, the frequency, beam current, beam hole radius, and beam radius were 280 GHz, 8.3 mA, 0.123 mm, and 0.041 mm, respectively. When the RF loss is 15 dB, which is close to the measured value, the gain is 16.5 dB. In contrast, for RF loss of 30 dB, it was 17.5 dB. Thus, even if the RF loss is doubled, the gain is only reduced by approximately 4 dB, and it is unlikely that the RF loss is the cause of the low gain of the prototype result. However, it is important to reduce the RF loss as much as possible when considering the gain and output.

Figure 17 shows the beam voltage dependence of the small-signal gain using the beam radius as a parameter. In this figure, the maximum SSG is 20.5 dB at a beam radius of $0.66r_d$ and 12.5 dB at a beam radius of $0.33r_d$. Thus, halving the beam radius results in a gain drop of approximately 8 dB.

Traditional helix TWTs, such as the Q/V band TWT, provide nearly 100 % beam transmission with a beam radius of 66 % of the beam hole radius. However, for the 300-GHz-band TWT, the beam radius is not clear owing to the effects of the manufacturing accuracy and thermal velocity. The effective beam radius can be close to $0.2r_d$ in an attempt to achieve good beam transmission. Therefore, it is speculated that the main cause of the low gain is the reduced coupling between the circuit wave and the electron beam owing to the small effective beam radius.

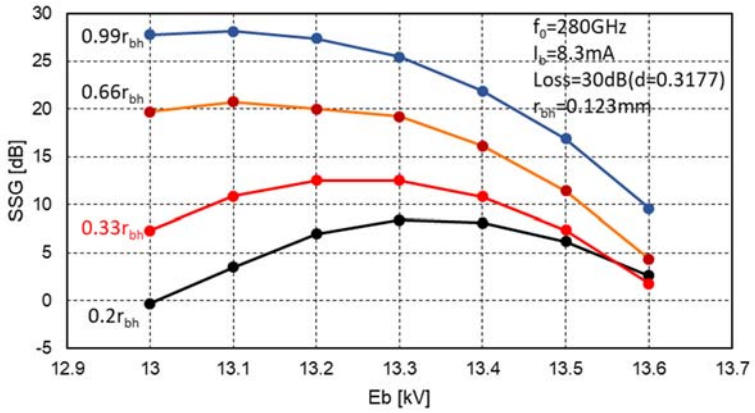

Figure 17. Small signal gain versus beam voltage for the beam radius as a parameter

5.4.2 Increasing interaction of FWG-SWS

It is estimated from the previous analysis that the cause of the low gain of the prototype TWT is the low coupling between the electron beam and the circuit wave, therefore, we analyse the interaction between the electron beam and the circuit wave in further detail to adopt new measures.

To increase the gain of FWG-SWS, we focused on the electron trajectory distribution when electrons passed through the electron beam hole of the FWG-SWS. While the effects of thermal velocity can be ignored for electron beams in the Q/V band, in the terahertz band TWT the electron beams are greatly expanded by it. This situation is illustrated in figure 18. In the figure, r_0 is the effective beam radius and r_{99} is Maxwell's velocity distribution when a velocity of 99 % is considered. The result of the beam spread by the thermal velocity for the PPM focusing electron beam calculated by the paraxial trajectory theory is shown in figure 19. The figure shows r_0 and r_{99} for the cathode magnetic field, B_c. The smaller the B_c, the greater the difference between r_{99} and r_0, and the spread due to the thermal velocity increases. Therefore, in the THz-band TWT, even if r_{99} increases, the difference between r_0 and r_{99} should be reduced to obtain a strong coupling between the electron beam and the circuit wave.

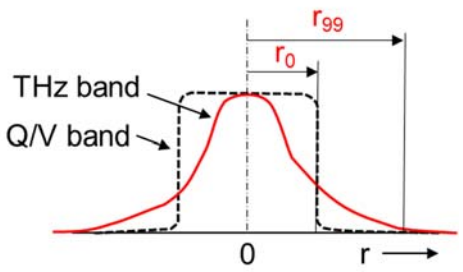

Figure 18. Radius vs Current distribution

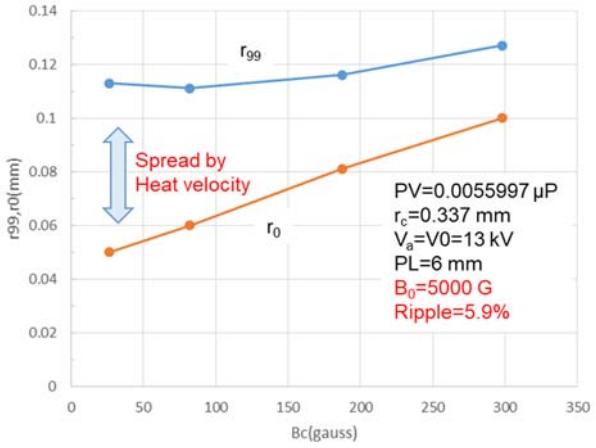

Figure 19. *r_0, r_{99} evolution vs Bc*

Further, in THz-band FWG-SWS, the RF electric field generated between pitches is expressed by equation (6)[6]. The TWT produces the gain by the interaction of the electric field and electron beam, as shown in figure 19a.

$$E_z(r) \propto \frac{\sin\left(\beta_e d/2\right)}{\beta_e d/2} \frac{I_0(\beta_e r)}{I_0(\beta_e r d)} \qquad (6)$$

In equation (6), d is the gap, βe (=2πf/u_0, u_0 is the electron velocity, f is the frequency) is the phase constant, and r_d is the electron beam hole radius.

Figure 20b shows the radius dependence of the RF electric field for the three types of beam hole radii. When the beam hole radius is as small as 0.05 mm, the decrease in the RF electric field near the central axis is small. However, it is difficult to realise an electron beam with a radius of 0.05 mm or less. When the electron beam hole radius is 0.1 to 0.123 mm, which corresponds to the design value, the RF electric field near the central axis decreases significantly.

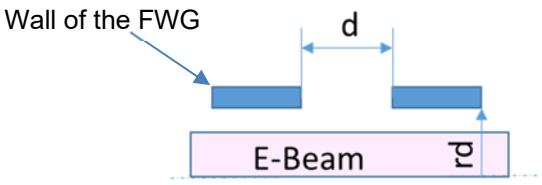

Figure 20a. Gap of FWG-SWS

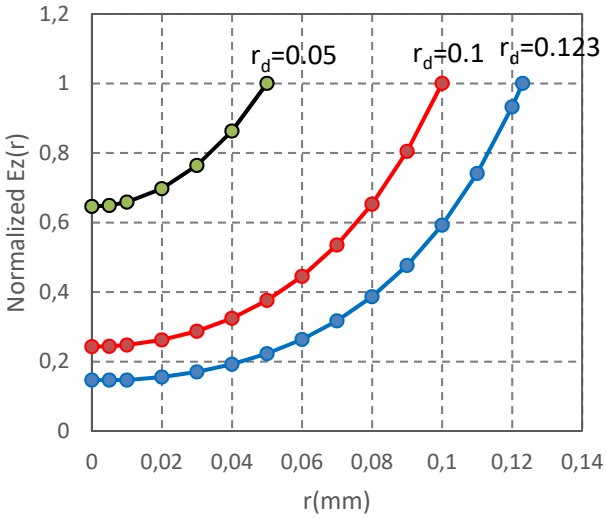

Figure 20b. $E_Z(r)$ dependency on r in gap

Next, we discuss the improvement in the electron density distribution in the electron beam. The electron beam travels in a straight line in the FWG-SWS and is then collected at the other side of the TWT device. Therefore, it is designed such that the electron beam can pass through the FWG-SWS. Previously, we designed a policy to increase the current by increasing the transmittance of the electron beam (figure 21(b)). The higher the current, the greater the gain. As a result of attempts to improve the electron beam transmittance, electrons were concentrated in the central part. However, the electric field of the RF signal becomes stronger around the wall of the electron beam hole (figure 21(c)); therefore, the interaction between the RF signal and the electrons is weakened. In figure 21(d), the shape of the electron beam flattens, and the electrons are distributed throughout the electron beam hole of the FWG. A higher gain is expected as the interaction increases. Figure 22 shows the current density distributions near the entrance of the electron beam hole of the TWT device in figure 10. The shape of the distribution is similar to that shown in figure 21(b), indicating a low interaction. Further, figure 23 shows the improved design of the TWT device. It is difficult to form a flattened current density distribution, and the current density distribution has two peaks. However, these peaks are located close to the electron beam hole wall, where the electric field strength becomes stronger implying that the interaction is expected to increase.

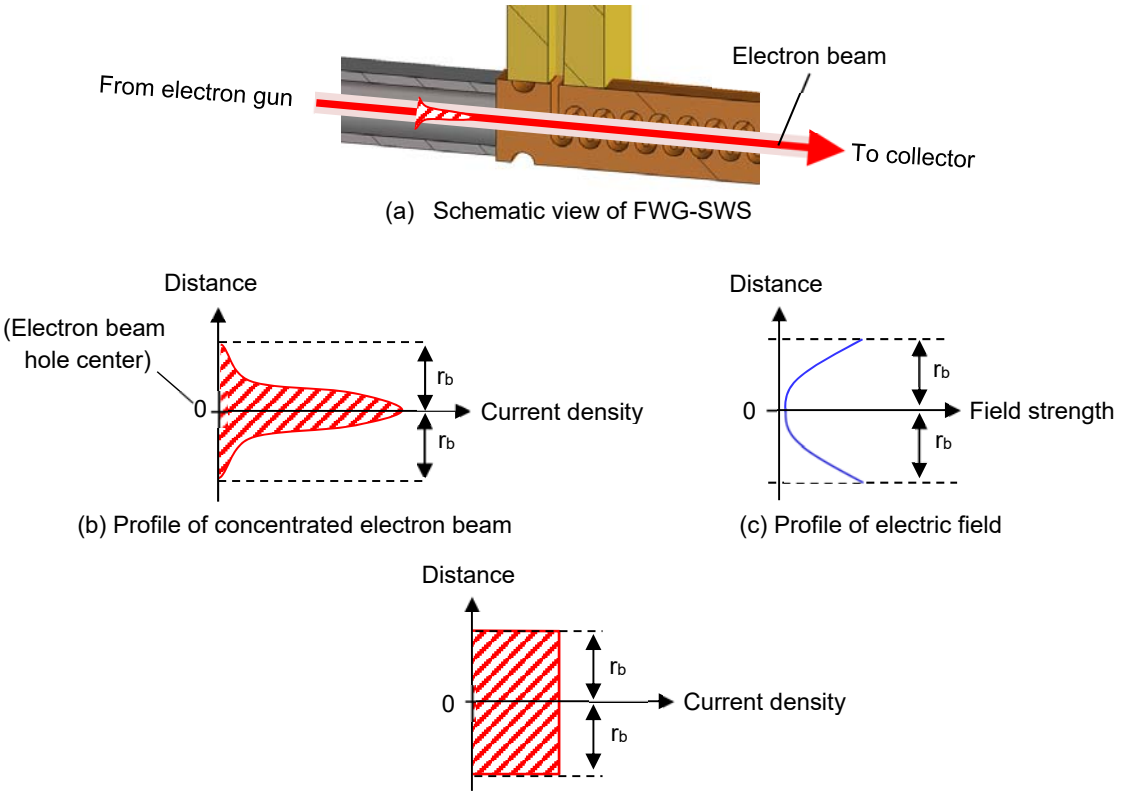

Figure 21. Electric field and centre focused electron beam.

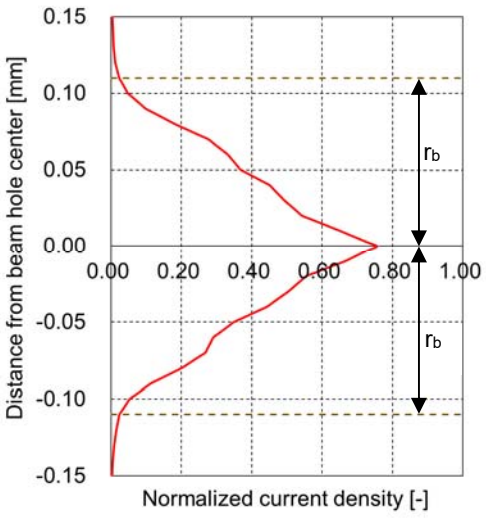

Figure 22. Current density (Previous design)

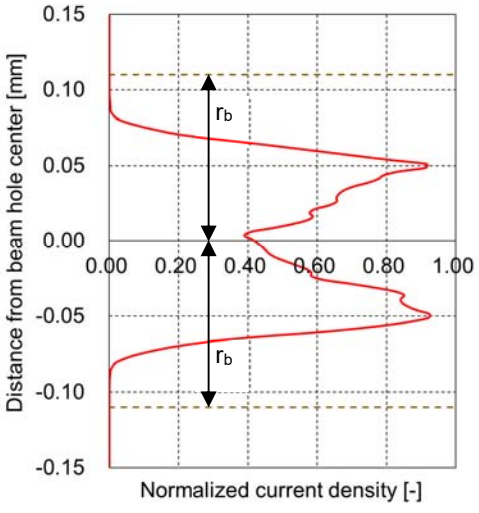

Figure 23. Current density (New design)

Next, a new design method for obtaining the current distribution shown in figure 23 is described. The transition region magnetic field distribution of the conventional electron gun, such as Q/V band TWT, was designed considering the outermost shell trajectory of the electron beam. However, in the case of

the THz-band TWT, because the electron beam is greatly expanded owing to the influence of the thermal velocity, the outer shell trajectory itself is unclear, and it is difficult to design the transition region magnetic field. Therefore, we propose a new transition region magnetic field for THz-band TWT which optimises the magnetic field distribution by focusing on the flattening of the current density distribution in addition to the maximum beam diameter and ripple rate of the outer shell electron beam trajectory.

Figure 24 shows the outermost electron trajectory and the axial charge density of the 300 GHz TWT electron gun when the magnetic field distribution is optimised to level the current density distribution using three types of cathode magnetic fields. The best electron beam is obtained when the cathode magnetic field is 0.02. The CST-PS was used for these simulations.

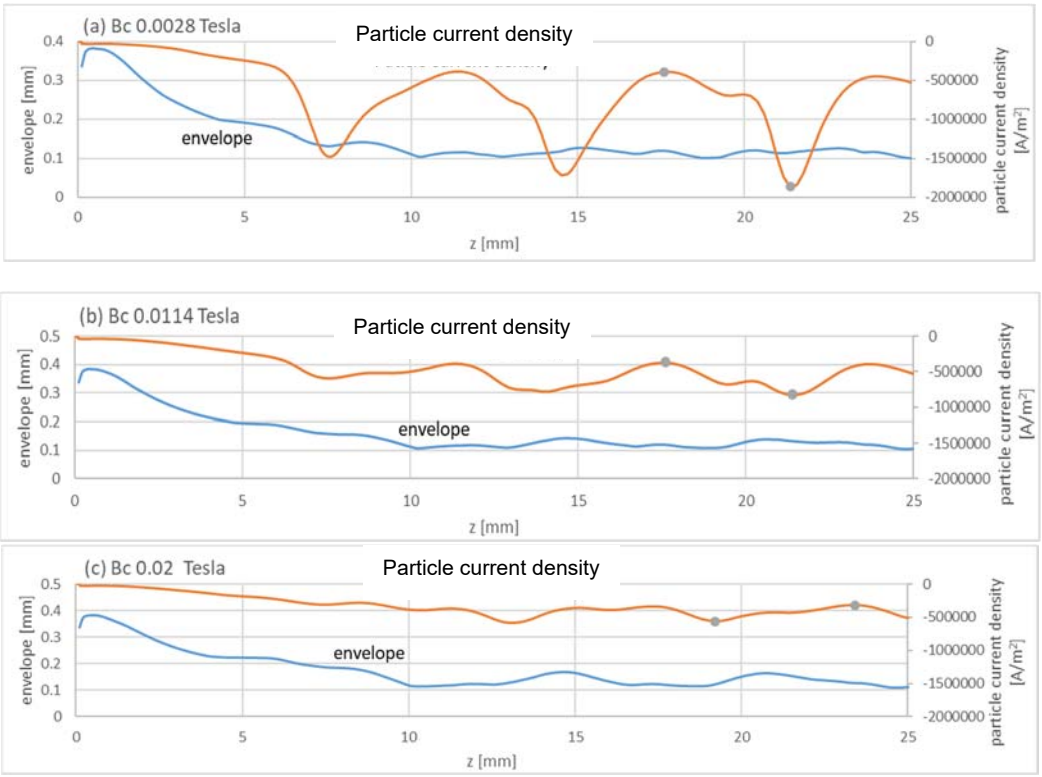

Figure 24. Electron density on axis and outermost shell electron trajectory (envelope) for 300-GHz-band TWT

Figure 25 shows the current density distribution of the electron beam cross-section at the positions where the charge densities are maximum and minimum in figure 23. When the value of B_C is small, the cross-sectional current distribution at the position where the charge density is maximised is concentrated on the side of the central axis.

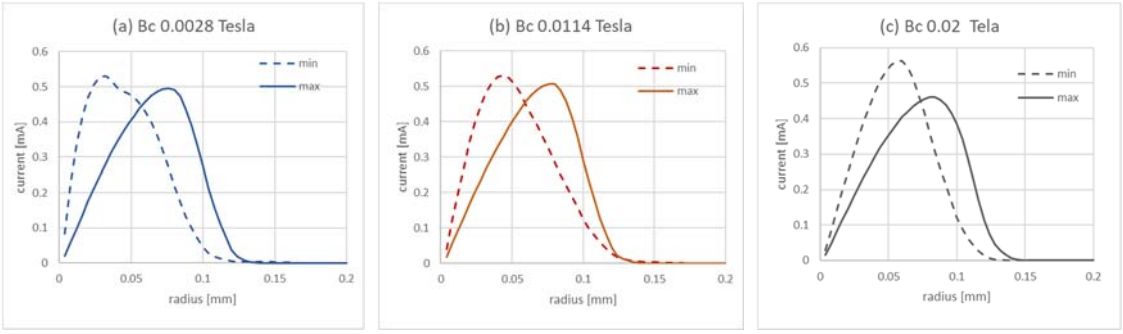

Figure 25. Current distributions at minimum electron density position and at maximum electron density position

For the three types of cathode magnetic fields, although 0.02 Tesla is the most suitable for B_C from the viewpoint of current distribution, 0.16 T is selected after considering the feasibility of the cathode magnetic field in the actual TWT. Figure 26a shows the electron beam trajectories when the magnetic field distribution is optimised for the outermost shell trajectory and the current density distribution at a B_C of 0.016 T. In figure 26a, 99 % of the electron beams pass through the beam hole of 0.123 mm. Figure 26b shows the magnetic field distribution in this case.

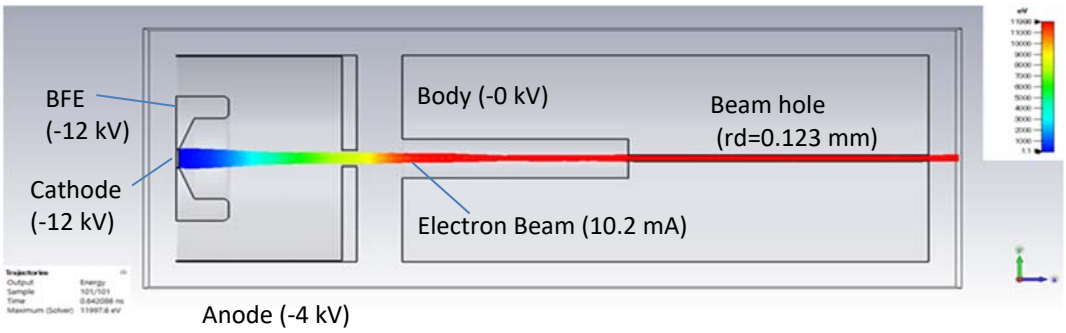

Figure 26a. Electron beam trajectories of electron gun for 300-GHz-band TWT

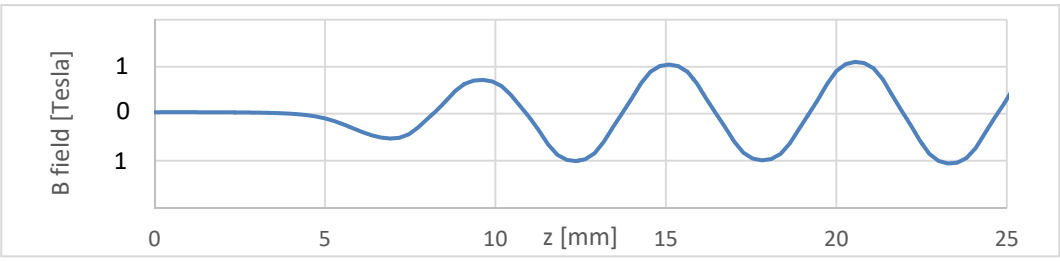

Figure 26b. Optimized magnetic field distribution in transition region

Finally, by adopting an electron gun designed by using the new design method that flattens the current density distribution introduced in this material, a strong coupling between the circuit wave and the electron beam is generated, thus, the gain of the TWT can be expected to increase.

5.4.3 Reduce RF transmission loss in the FWG-SWS

Second, we attempted to reduce the manufacturing error of the FWG-SWS. The previous FWG-SWS was divided at the centre of the FWG and the depth of the FWG could reach approximately 300 μm. Therefore, the two parts were laminated via diffusion bonding. Further, the transmission loss is primarily caused by the alignment error of the fabrication, thus, we improved the MEMS manufacturing process and fabricated an FWG-SWS with an 'unsplit' FWG.

Moreover, by reducing the degradation of electrical properties caused by manufacturing errors, the performance of the FWG-SWS can be brought closer to the microwave theory to achieve a higher gain. The TWT device prototype shown in Section 5.1, used the FWG-SWS created in two parts with FWG-SWS divided at the centre, as shown in figure 27, because its structure is too complex to create the FWG and the electron beam hole together with very high precision. We used the X-ray LIGA process, and its exposure process was conducted at SPring-8 which is a large synchrotron radiation facility in Japan. SPring-8 delivers the most powerful synchrotron radiation currently available. The parts were laminated by diffusion bonding. Here, two factors degrade the performance of FWG-SWS, mechanical alignment error and deformation caused by high pressure during the diffusion bonding process. The RF transmission characteristics are susceptible to small alignment errors and when deformation occurs after diffusion bonding, the cross-sectional shape of the circular hole becomes elliptical. The differences between the maximum and minimum diameters (roundness) of the electron beam holes exceeded 20 μm. Thus, the number of electrons passing through the electron beam hole decreases because the cross section of the hole decreases. Figure 28 shows the gain of the TWT simulated by the CST studio suite. The effect of the alignment error is greater on the gain than on the deformation of the electron beam hole.

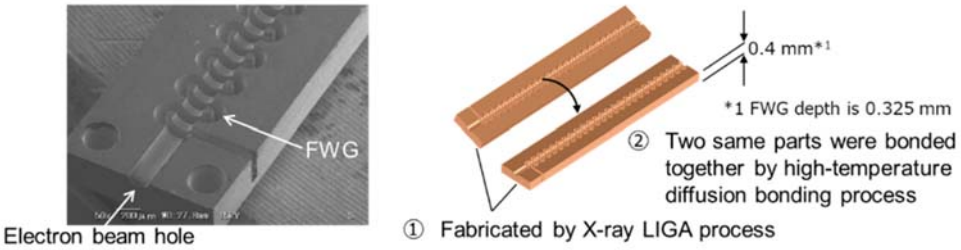

Figure 27. Manufacturing process of previous FWG-SWS.

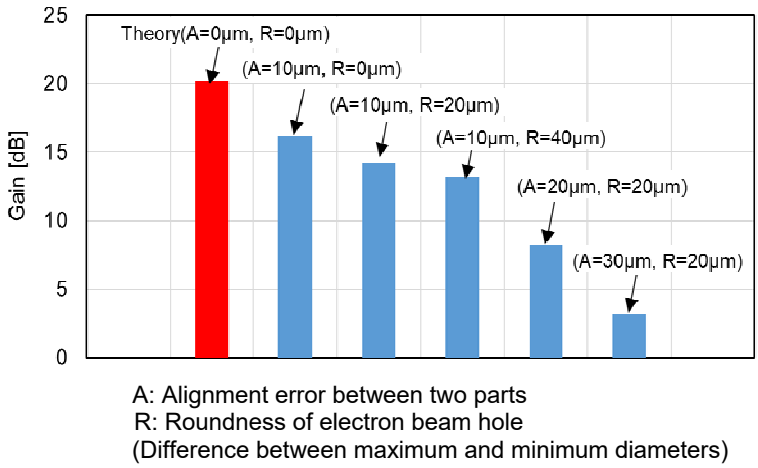

Figure 28. Gain reduction caused by manufacturing error. （The accuracy of the manufacturing process used in this prototype is close to the theoretical value highlighted in red.）

To solve this problem, we improved the manufacturing process of FWG-SWS. In this method, the main body, including the waveguide, is made in one piece, as shown in figure 29. The main body was fabricated using the X-ray LIGA process, except for the electron beam hole. An electron beam hole with a diameter of 200 μm was formed by precision machining after the LIGA process. Subsequently, the body was laminated with a top plate via low-temperature diffusion bonding. Surface roughness (Sa) of the wall of the FWG-SWS ranges from 0.06 to 0.07 μm, while that of the previous FWG ranged from 0.17 to 0.43 μm. There is no exit alignment error in the FWG. The roundness of the electron beam holes was below 20 μm.

The electron beam hole is a through-hole, but if a long drill with a small diameter is used to form the electron beam hole, the drill will break. Thus, to avoid breaking, a drill is used to process from both directions to form the through-hole. In this machining method, misalignment occurs at the tip of the hole, which increases the loss of RF waves. We evaluated drilling from one direction and formed a through-hole. From the next prototype, FWG-SWS was manufactured using the one-direction method. This is expected to reduce the loss of the RF wave propagating in the FWS-SWS.

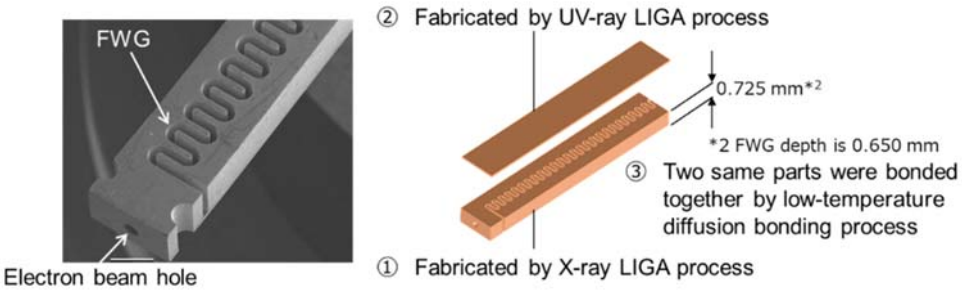

Figure 29. Improved FWG-SWS.

6 TWT DEVICE PROTOTYPING

We designed the improvements, as described in Section 5.4. A TWT device prototype is fabricated using a single FWG-SWS. Currently, we are proceeding with electrical adjustments of the TWT device prototype in the configuration shown in Figure 30. An aging process was also conducted. Here, we present an interim report on the evaluation results obtained so far.

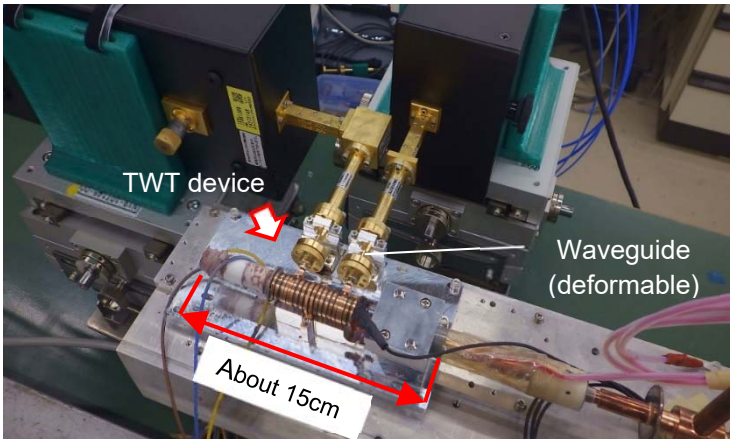

Figure 30. Photo of the 4th prototype TWT experimental set-up.

Figure 31 shows the electron beam characteristics in the pulse mode of the TWT device prototype. In the figure, the anode voltage is the design value of 8 kV, and a cathode current of 10.8 mA is obtained. The performance calculated from the above values is 0.015×10^{-6} $A/V^{3/2}$, which is almost consistent with the simulation results. In addition, the cathode, collector, and body current were approximately 9.5, 10.8, and 1.3 mA, respectively, while the beam transmittance was 90 %. This value is not yet sufficient for the target, but it is a significant improvement over the previous prototype results.

In the TWT device prototype, a new design method using CST-PIC was introduced to improve the electron beam transmission characteristics, and an optimum design was carried out. In addition to indicating that the design change was effective, it is necessary to indicate that the RF characteristic measurement value is close to the design value. However, the most important factor that indicates that the design is effective is the electron beam transmittance. The electron beam system is at the level at which the gain target can be achieved.

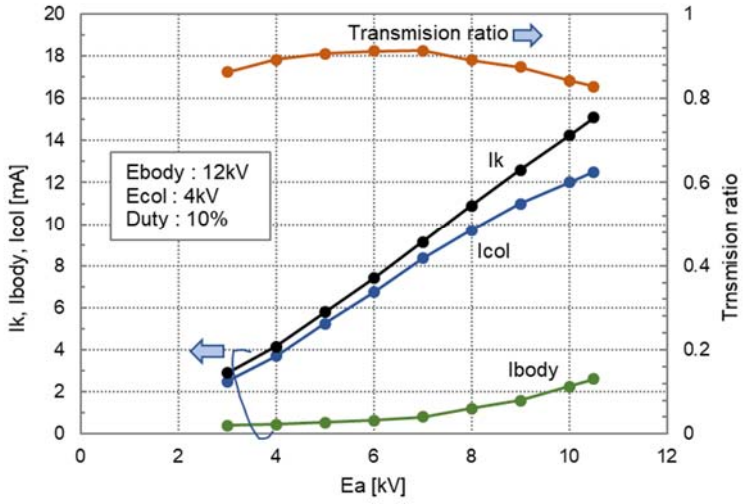

Figure 31. Electron beam characteristics of the 4th prototype TWT.

Figure 32 shows the frequency dependence of S21 (RF loss) of the TWT device prototypes in the cold state without flowing the electron beam. By implementing measures to reduce RF loss, as described in Section 5.4.3, at approximately 290 GHz, an RF loss of approximately -16 dB is expected with consideration of the -4 dB RF loss of the input/output circuit. The RF loss of -16 dB was close to the simulation value. In figure 32, the back line shows the data of the best characteristics of the TWT devices produced so far. The black line is close to the simulated results obtained using CST. However, the 4th prototype result was lower than the 1st prototype result. However, because the machining accuracy of the electron beam hole is insufficient, the RF loss in the region below 285 GHz is − -20 dB or less.

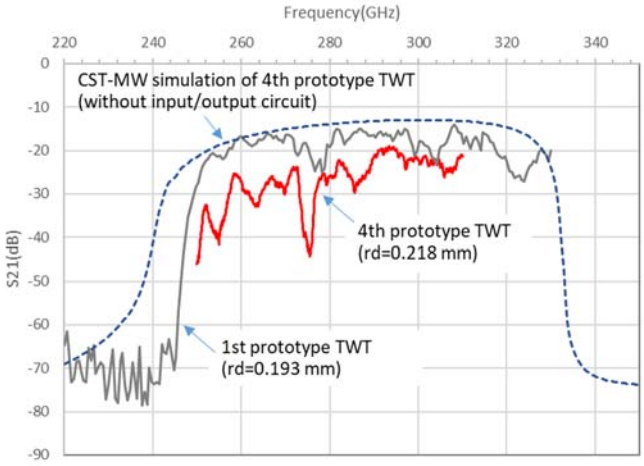

Figure 32. S21 of the 4th Prototype TWT (Cold).

Figure 33a shows the frequency characteristics of S21 (TWT device gain) under hot conditions (electron beam was on). Unfortunately, the RF gain is below 0 dB, and the frequency with respect to peak gain varies in synchronisation with the operating voltage. The frequency of the peak gain moved to the left when the applied voltage increased. Further, the peak value of the gain decreases as the frequency increases because of the synchronisation shift (coupling theoretically weakened). At approximately 290

GHz, the RF gain is approximately 10 dB. This is due to the large RF loss and weak coupling between the beam and RF waves.

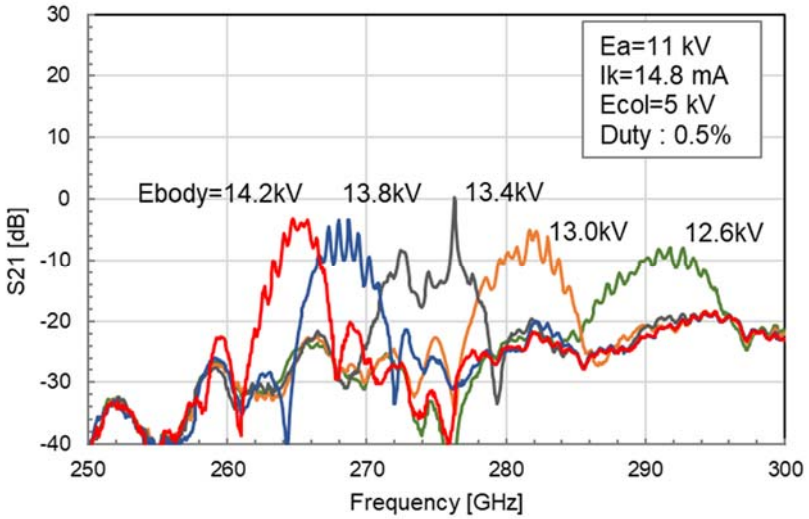

Figure 33a. S21 of the 4th prototype TWT (Hot conditions).

To analyse the cause of the negative gain in figure 33a in further detail, the value (i.e., an approximate net gain) obtained by subtracting the RF loss value in figure 32 from the value of S21 in figure 33a is shown in figure 33b. Figure 33b shows that a gain of 20 dB or greater was obtained without RF loss. If the RF loss is close to the actual value of -16 dB of the 1st prototype, it is estimated that a gain close to 10 dB was obtained. In figure 33b, a strong resonance is observed at frequencies around 275 GHz. This is inferred to be due to the reflections of the machining accuracy of the electron beam hole.
In the future stage of production, measures should be taken to prevent ossification due to an increase in gain.

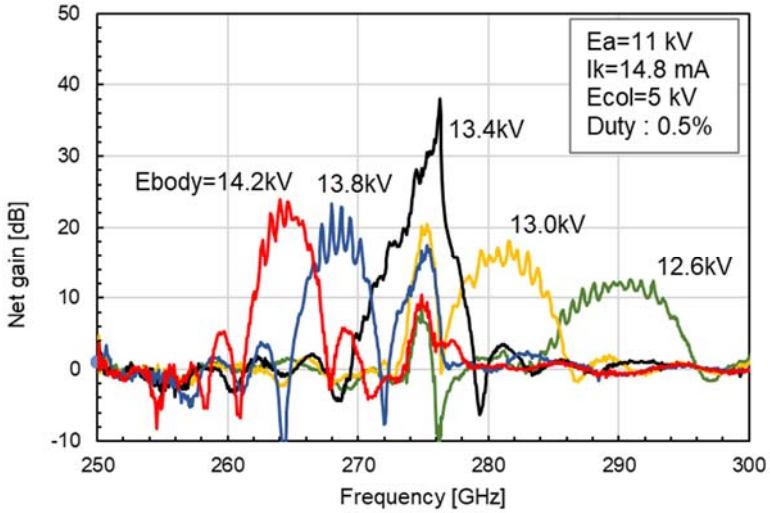

Figure 33b. Frequency characteristics after FWG loss correction (pulse).

In figure 32a, the gain of the TWT device prototype did not reach the target value. However, we believe that if we improve the processing accuracy of the electron beam hole and reduce the RF loss, the target value can be achieved.

Currently, electrical adjustment in the cw mode is proceeding. Under conditions of cathode currents of 10 mA (CW) and body voltage of 12 kV, an electron beam transmittance of approximately 76 % was achieved. This result indicates that the target value can be achieved using the next prototype.

7 HOW TO ACHIEVE WIDEBAND TWT device

Inside the TWT, interactions occur when the phase velocity of the RF signal wave and the speed of the electron beam are approximately the same. In addition, if it can be synchronised with the electron beam in a small region of velocity dispersion, the operating frequency band can be widened. In figure 3, this is achieved by expanding the region wherein the ω-β curve and the straight line of the operating voltage E_b cross or are close. This implies that setting a large value of (βp) sync in the ω-β diagram is necessary to ensure that the circuit wave is synchronous with the electron beam. However, setting a large value of (βp)sync results in a lower coupling impedance and a low gain. In contrast, if a sufficient gain can be secured, it is possible to realise a wide band of TWT. Therefore, here, we discuss measures to ensure sufficient gain in the 300 GHz TWT.

We introduce Pierce's gain parameter C to discuss the gain of TWT. C is given by the ratio of the coupling impedance and electron impedances.

$$C = \left(\frac{1}{4}\frac{Z_c}{Z_b}\right)^{1/3} = \left[\frac{1}{4}Z_c\left(\frac{I}{V}\right)\right]^{1/3} \qquad (7)$$

where Z_b is the beam impedance, I is the beam current, and V is the beam voltage. Z_c is the coupling impedance, which is strictly defined by the following equation

$$Z_c = \frac{\int_0^b E_z^2(r)2\pi r dr}{2\beta^2 P} \qquad (8)$$

where, E_z is the z component of the RF electric field, β is the phase constant, and P is the electromagnetic power flow. The gain of the TWT depends on the gain parameter C given by equation (7), RF loss, and circuit length (wave number). To reduce the RF loss of the FWG-SWS, it is necessary to develop a technology that precisely bonds parts. The divided FWG-SWS for lengthening the circuit was evaluated to increase the gain, as described in Section 5.3.

To increase the gain, it is necessary to adopt measures to reduce RF loss and lengthen the circuit length, but before that, it is more important to adopt measures to increase the gain parameter given by equation (7). The following items can be considered as measures to increase the gain from equations (7) and (8):

(1) Optimisation of electron beam shape
(2) Lower beam impedance.
(3) Increase in the RF electric field intensity

The countermeasure of Item (1) is proposed in Section 5.4. In addition, items (2) and (3) are also very important countermeasures, but both will degrade the beam transmission. However, if sufficient gain cannot be obtained by the measures of item (1), it may be necessary to consider items (2) and (3) even if the deterioration of the beam transmittance is tolerated. If the value of the gain parameter can be increased employing the above countermeasures, the gain of the TWT can be increased. Furthermore,

we should know that the increase in the gain parameters can contribute to further expanding the bandwidth of the TWT gain.

8 Conclusion

This deliverable provides the results of a theoretical study of TWT devices and prototyping. The results of the design changes were sufficiently effective. By reducing the RF loss of the FWG-SWS, it is possible to achieve the target value of the gain. The state-of-art mechanical processing is precise enough to fabricate THz TWTs, however, still we have some challenges in assembly processes and device configurations. In future prototyping, we will use an improved process for fabrication of the electron beam hole. Now, the hole is formed by drilling step by step from both sides, due to damage of drill blades. This process causes mechanical misalignment in the hole diameter. In the next prototype, the electron beam hole will be machined from one side, to reduce the diameter change of the electron beam hole and the high frequency loss.

9 References

[1] N. Kosugi, D. Matsumoto, T. Machida, T. Munehiro, Y. Mori, T. Stewart, “Q/V-band Helix TWT for Future High Throughput Satellite Uplink Applications,” International Conference on Vacuum Electronics (IVEC), 2020.

[2] N. Masuda, M. Yoshida, K. Okamoto, “Development Activity of 0.1/0.3 THz Power Module,” International Conference on Energy, Materials, Nanotechnology (EMN) Meeting on Terahertz, pp. 4-5, 2017.

[3] K. Tsutaki, Y. Neo, H. Mimura, N. Masuda, M. Yoshida, “Design of a 300 GHz TWT with a Folded Waveguide Fabricated by Micro electro mechanical Systems,” J Infrared Milli/THz Waves, **37**, 1166–1172, 2016. DOI 10.1007/s10762-016-0306-5.

[4] G. Dohler, D. Gagne, D. Gallagher, R. Moats, “Serpentine Waveguide TWT,” International Electron Devices Meeting (IEDM), pp. 485-488, 1987.

[5] J. E. Rowe, “Nonlinear Electron-Wave Interaction Phenomena,” Academic Press, New York, United States, 1965.

[6] A. S. Gilmour Jr., “Principle of Traveling wave tubes,” Artech House, Norwood, Massachusetts, United States, 1994.